Optical study on the phase transition of lead lanthanum zirconate titanate $Pb_{0.92}La_{0.08}(Zr_{0.70}Ti_{0.30})_{0.98}O_3$ ceramics

J. Kobayashi
Kagami Memorial Laboratory for Materials Science and Technology, Waseda University, 2-8-26 Nishi-Waseda, Shinjuku-ku, Tokyo 169, Japan and Research Development Corporation of Japan, 2-5-2 Nagata-cho, Chiyoda-ku, Tokyo 100, Japan

T. Asahi, M. Ichiki, K. Saito, T. Shimasaki, H. Yoshii, and Y. Itagaki
Kagami Memorial Laboratory for Materials Science and Technology, Waseda University, 2-8-26 Nishi-Waseda, Shinjuku-ku, Tokyo 169, Japan

H. Ikawa
Department of Chemical Technology, Kanagawa Institute of Technology, 1030, Shimo-Ogino Atsugi-city, Kanagawa 243-02, Japan
(Received 27 June 1994; revised manuscript received 14 September 1994)

Optical gyration G, birefringence Δn, and their electric-field E dependences of transparent ceramics of $Pb_{0.92}La_{0.08}(Zr_{0.70}Ti_{0.30})_{0.98}O_3$ were studied by using high accuracy universal polarimeter in a temperature range between -10 °C and 90° C. The high-temperature phase manifested neither spontaneous nor induced G by applying the biasing E, while the low-temperature phase did characteristic hysteresis loops of G, and Δn with respect to E. Group-theoretical consideration of gyro-optical properties of both phases led us to the conclusion that the high- and low-temperature phases are cubic T_h and trigonal C_3. They transform into each other at $T_c = 10.3$ °C with essentially second but apparently first order. The free-energy function which drives the transition was determined by using electro-optic phenomena occurring in the phase-transition region. Calculated and observed values of G and Δn as a function of E were in excellent agreement in the transition region. However, they began to deviate from 50 °C and the deviations became serious above 80 °C. Brief comments are given on the anomalous dielectric behavior of lanthanum modified lead zirconate titanate ceramics.

I. INTRODUCTION

A lanthanum modified lead zirconate titanate (PLZT) group was first fabricated by Haertling and Land[1] as transparent ceramics. They are distinguished in exhibiting large electrooptic effects. In addition to this practical applicability, they have been attracting a great interest for their complicated characteristic dielectric property. For example, the dielectric nature of some PLZT, which was cooled with and without electric fields E, was markedly different.[2] Spontaneous polarizations did not occur at a temperature where the initial dielectric constants ε became maximum. In order to explain such anomalous dielectric properties, various ideas were already put forward. Keve and Bye[3] proposed a two-phase model, Meitzler and O'Bryan[4] a polymorphic model, Carl and Geisen[5] local ordering models, etc. Although these early studies shed light on some aspects of physics of PLZT, convincing interpretations consistent with most of the dielectric phenomena could not be obtained. Recently Viehland, Li, Jang, Cross, and Wuttig[6] proposed a cluster model. This model seems interesting in that it is based on nanoscale electron-microscopic findings[7] of microdomains on the one hand, and is reminiscent of superparamagnetism[8] on the other.

Although huge numbers of active works have been accumulated so far, it is surprising to us that most basic problems of PLZT have still been left unsolved. For example, the crystal classes of both high- (H) and low- (L) temperature phases of a PLZT family are not clearly known. Optical birefringences Δn were measured under various conditions, but there exist no reports for optical activity (OA). As structural and optical evidence is indispensable for elucidating dielectric properties and phase changes of a crystal, it seems that more detailed studies on these directions are keenly awaited.

We invented a high accuracy universal polarimeter (HAUP),[9-11] which enables us to measure OA, Δn, and the rotation of the indicatrix of solids of any symmetries. Therefore it was tempting for us to apply it to optical study on PLZT. The crystal class of the prototype form of $PbTiO_3$, $PbZrO_3$, and their solid solutions has been known to be O_h. Among the ferroelectric subgroups of O_h, which can be realized as L phases, say, C_{2v}, C_{3v}, C_{4v}, only orthorhombic C_{2v}, must be optically active. However, as will be described later, the OA of the C_{2v} phase will be lost when the specimens of this class are fabricated in a ceramic state. Thus if the L phase of PLZT is found optically active, an essential revision might be made to the previous concepts of PLZT. Thus measurements of OA seemed very crucial. Many groups[12] already measured Δn of PLZT. The HAUP method also has an ability of measuring Δn more accurately than the existing compensator methods.

We revealed OA, electro-optic, and electrogyration effects of ceramics with a composition of $Pb(Zr_{0.70}Ti_{0.30})O_3$ with the addition of 8 mol% La_2O_3 (abbreviated usually as 8/70/30) by HAUP experiments. We also examined the crystal structures of the H and L phases by using x-ray-diffraction methods. This paper reports these optical and structural data and an interpretation of the phase transition elucidated from them.

II. HAUP MEASUREMENTS

Original powders of the specimens were obtained by using a multistep precipitation method. The phase diagram of PLZT with the present composition was first determined by Haertling and Land,[1] as is reproduced in Fig. 1. Here T_m designates the temperature where ε showed a broad peak, and T_d the temperature below which the ferroelectric phase could exist. T_d differs considerably from that determined by us, as will be seen afterward.

A perfectly transparent specimen, 2600 μm long, 285 μm wide, and 28 μm thick, was prepared by careful polishing with Al_2O_3 powders of homogeneous grain size of 0.2 μm. E were applied along the width through the electrodes of evaporated gold. Light struck normally upon the surfaces of the specimen, the direction of the beam then being perpendicular to E.

HAUP measurements were carried out on the sample placed in a vacuum chamber and held at various temperatures between $-10\,^{\circ}C$ and $90\,^{\circ}C$ within an accuracy of $\pm 0.02\,^{\circ}C$. The light source was a He-Ne laser with a wavelength of 6328 Å. $B(0)$, retardations Δ, and characteristic angles θ_0 in the HAUP method[9,10] were measured. These quantities are related by

$$B(0)=(\gamma-2k)\sin\Delta+2\delta\Upsilon\cos^2(\Delta/2)\ , \tag{1}$$

or equivalently,

$$B(0)/\sin\Delta=\gamma-2k+\delta\Upsilon\cot(\Delta/2) \tag{2}$$

and

$$\theta_0=-\tfrac{1}{2}(p+q)\cot(\Delta/2)-\tfrac{1}{2}\delta\Upsilon+\psi\ . \tag{3}$$

Here k represents the ellipticity of the elliptically polarized wave traveling in the specimen, and ψ is the rotation angle of the indicatrix. $\gamma=p-q$ and $\delta\Upsilon$ are the principal systematic errors; p and q designate the parasitic ellipticities of the polarizer and analyzer, respectively, and $\delta\Upsilon$ is the deflecting angle from the accurate crossed Nicols condition. The measuring temperature range included the paraelectric, intermediate, and ferroelectric phases.

Here the HAUP measurements at 20 °C will be described as a typical example. In order to obtain γ, the reference crystal method[11] was adopted, by taking a $LiNbO_3$ crystal as the standard one. From this optical system $\hat{p}$ was obtained as -2.8×10^{-4}. Dependencies of $B(0)$, $\Delta/2$, and θ_0 on E are shown in Figs. 2(a)–2(c). Here the solid circles represent the values measured in the process of applying biasing E from a positive to negative direction, while the open ones values for the reversed one. From Figs. 2(b) and 2(c), the linear relation between θ_0 and $\cot(\Delta/2)$ was obtained as indicated in Fig. 3(a). From the derivative of the line, $\hat{p}+q=1.4\times10^{-4}$ was obtained. As $\hat{p}$ was already obtained, $\gamma=\hat{p}-q$ was immediately calculated as -7.0×10^{-4}. Here it was seen that ψ did not depend on E. It would become clear afterwards that ψ was zero, since both phases were determined to be optically uniaxial. The relation between $B(0)$ and Δ is indicated in Fig. 3(b), where

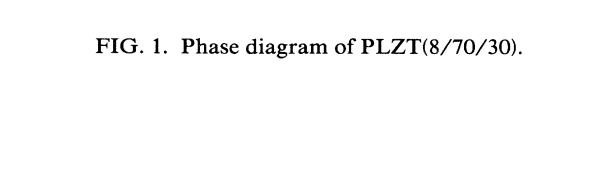

FIG. 1. Phase diagram of PLZT(8/70/30).

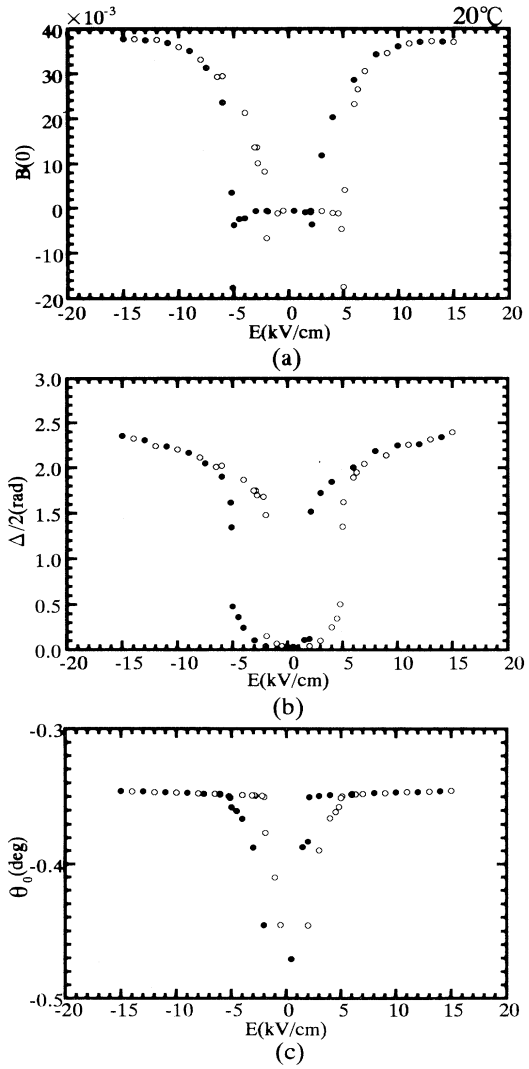

FIG. 2. E dependences of (a) $B(0)$, (b) $\Delta/2$, and (c) θ_0 of PLZT(8/70/30) at 20 °C.

$\delta\Upsilon = -2.5\times10^{-4}$ was derived from the value of $B(0)$ at $\Delta=0$ as can be definitely seen in the inset of the enlarged scales. As the systematic errors of γ and $\delta\Upsilon$ were thus obtained, E dependences of Δn and G were acquired as shown in Fig. 4(c).

E dependences of Δn and G at typical temperatures are shown in Fig. 4. Below about 10 °C, Δn and G manifested typical butterfly-type hystereses which feature the ferroelectricity of this phase. In the temperature range between about 10 and 20 °C, the butterfly loops of Δn split into two, say, high and low value branches. This fact was indicative of the presence of an intermediate state in a process of polarization reversal. However, it was a remarkable fact that G appeared only above a threshold value of E and disappeared below another characteristic field, thus forming a characteristic hysteresis. In the temperature range from about 21 to 60 °C Δn were induced quadratically and were saturated at higher E values. However, above about 61 °C the induction of Δn became small and almost in a linear manner. Above 80 °C, it was severely suppressed. On the other hand, G manifested hysteresis behavior until nearly 60 °C. They faded away perfectly above the vicinity.

III. CHANGE OF SYMMETRY

A. X-ray study

In order to obtain information of the symmetries of the H and L phases, we used x-ray-diffraction methods at first. Debye-Scherrer photographs of a ceramic specimen at room temperature indicated that it consisted of powder texture of crystallites although the diffraction lines were rather spotty. On the other hand, a specimen, which was cooled to 0 °C under a biasing field of $E=20$

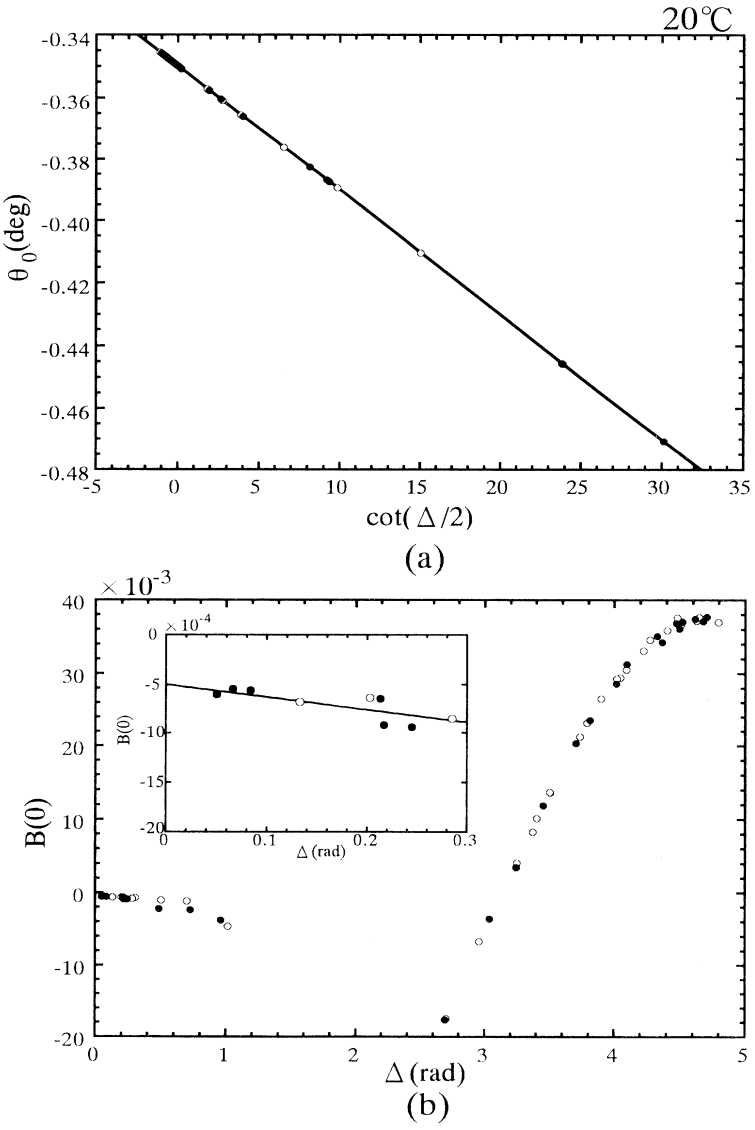

FIG. 3. Relation of (a) θ_0 with respect to $\cot(\Delta/2)$, and (b) $B(0)$ with respect to Δ of PLZT(8/70/30) at 20 °C.

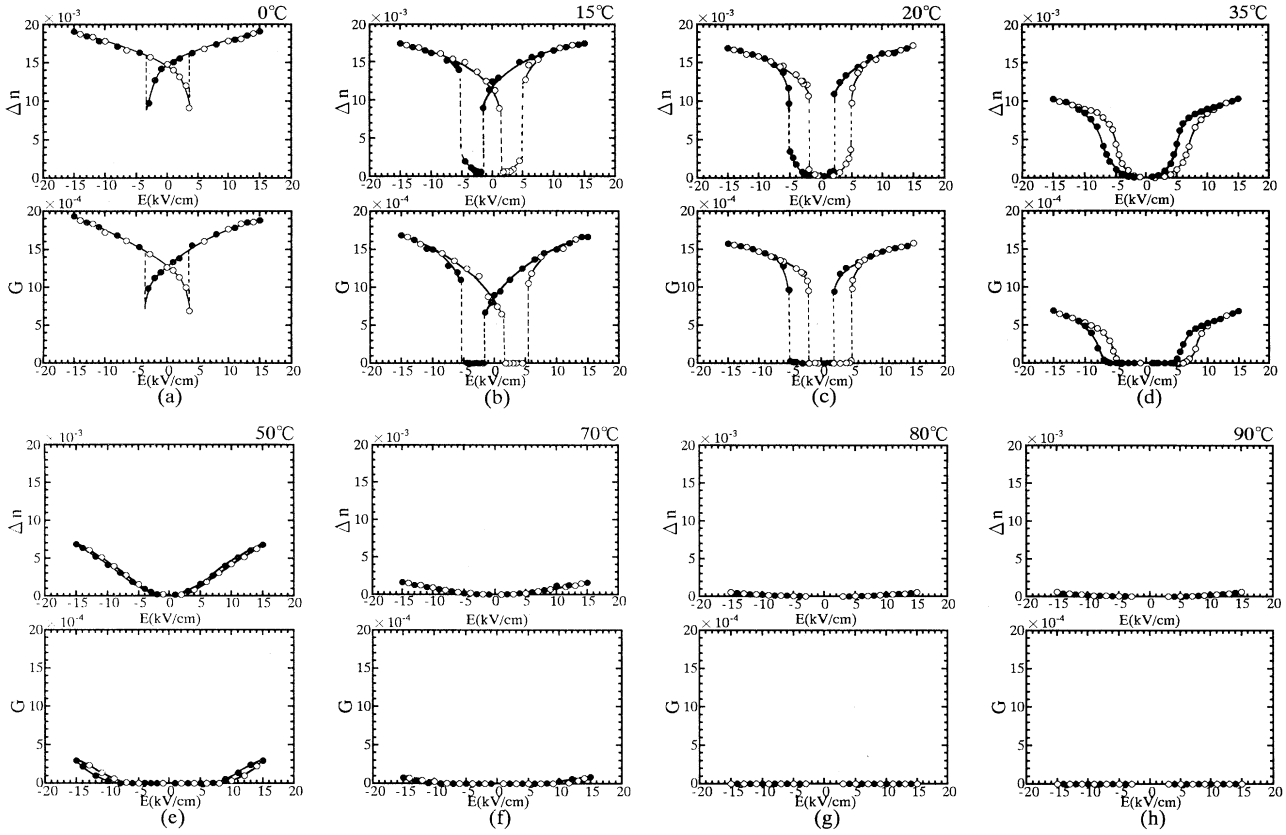

FIG. 4. E dependences of Δn and G of PLZT(8/70/30) at typical temperatures between 0 and 90 °C.

kV/cm, produced almost similar Debye-Sherrer rings except a slight broadening of the 431 spectrum. In order to obtain more detailed evidence concerning splitting of spectra and structure of powder texture, the Weissenberg method with a camera radius of 28.648 mm was applied to a long platelike specimen, 360 μm wide (electrode distance), and 56 μm thick. The specimen was rotated around the long axis, to which E was normally applied. The specimen was covered by a beam limiter with the slot width of 300 μm, which selected only the zero-layer spectra. Weissenberg photographs taken at 90 °C without E are shown in Fig. 5(a). It was found that the diffraction

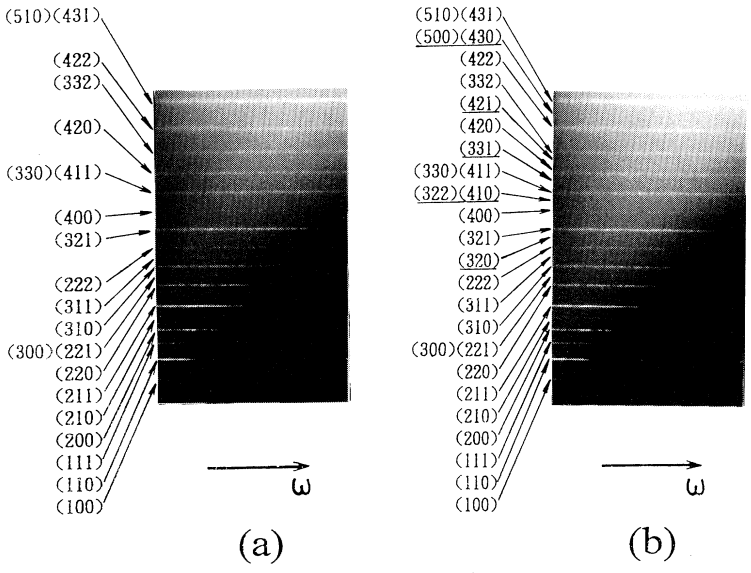

FIG. 5. Weissenberg photographs of PLZT(8/70/30) at (a) 90 °C and (b) −30 °C.

spectra appeared as straight lines parallel to the ω axis of a Weissenberg chart.

As the H phase of PLZT certainly has a perovskite structure, it was natural to expect that the spontaneous polarization in the L phase will occur along any of (i) [001] or (ii) [110], or/and (iii) [111] directions. If the specimen of the Weissenberg photograph was purely a single crystal in the L phase, only the following groups of spectra would appear: $(h0l)$ and $(0kl)$ spectra for the (i) case, spectra of $h=\pm k$ for the (ii) case, and spectra of $h=l$ and $2k=h+l$ for the (iii) case. The photograph of the specimen at -30 °C after field cooling of 15 kV/cm is shown in Fig. 5(b). It was remarkable there that the spectra did not obey any of the above selection rules at all, and were the same as those expected to appear in the powder photographs. All the spectra observed in Figs. 5(a) and 5(b) are collected in Table I. This fact indicated that the orientation of the constituent crystallites was distributed almost equally in all the Eulerian angles in the space. In this case the locus of the same reciprocal points of the crystallites forms a sphere of radius of $1/d_{hkl}$, intersecting with the zero-layer reciprocal plane at a circle of the same radius. This is the reason, of course, why the spectra appeared as the lines in the Weissenberg photographs. Every spectrum line in Figs. 5(a) and 5(b) was homogeneous in its optical density. This fact confirmed the homogeneous distribution of the crystallites more definitely. Splittings of spectra reported by Keve and Bye[3] and Yokosuka and Marutake[13] were not observed. The outstanding change of Fig. 5(b) from 5(a) photographs was a sudden increase of the intensities of the following cubic spectra: 320, 322(410), 331, 421, 430(500), overlapped spectra being indicated by parentheses. These spectra underlined in Fig. 5(b) were clearly discernible, although missing in Fig. 5(a). This phenomenon led us to infer that sudden shifts of Ti and Zr atoms would take place in the L phase from the special positions in the H phase, although the accompanying deformation was small.

TABLE I. Spectra observed in Weissenberg photographs of PLZT at (a) 90 °C and (b) -30 °C.

	d_{hkl} (Å)	
(hkl)	(a)	(b)
(100)	4.12	4.13
(110)	2.89	2.92
(111)	2.36	2.34
(200)	2.06	2.04
(210)	1.84	1.85
(211)	1.68	1.68
(220)	1.46	1.45
(221)(300)	1.38	1.38
(310)	1.31	1.30
(311)	1.24	1.24
(222)	1.19	1.19
(320)		1.15
(321)	1.10	1.10
(400)	1.03	1.03
(410)(322)		1.00
(411)(330)	0.97	0.97
(331)		0.94
(420)	0.92	0.92
(421)		0.90
(332)	0.88	0.88
(422)	0.84	0.84
(430)(500)		0.83
(431)(510)	0.81	0.81

The diffraction intensities I of Weissenberg lines at 90 °C of PLZT (8/70/30) was calculated by the formula

$$I(hkl)=K|F|^2pLm_k \exp\left\{-B\left[\frac{\sin\theta}{\lambda}\right]^2\right\}, \quad (4)$$

where K is the scaling factor, F the structure factor, p the polarization factor, L the Lorentz factor, m_k the multiplicity, and B the isotropic temperature factor. All atoms were assumed to take the following special positions: Zr and Ti at $(\frac{1}{2},\frac{1}{2},\frac{1}{2})$, Pb and La at (0,0,0), and O at $(\frac{1}{2},\frac{1}{2},0)$, $(\frac{1}{2},0,\frac{1}{2})$, and $(0,\frac{1}{2},\frac{1}{2})$. K and B were determined from the observed intensities I^{ob} by plotting $\ln(I^{ob}/|F|^2pLm_k)$ with respect to $\sin^2\theta$; thus $K=1.104\times10^{-4}$ and $B=1.328$ Å^2. Here the conventional residual factor R expressed by I^{ob} and calculated intensity I^{cal} reached 5.41%. Subsequently we evaluated the change of R values due to the shifts of the Ti and Zr group along the aforementioned three directions (i)–(iii). As shown in Fig. 6, R values showed minima at the different amounts of shifts χ in each case: $\chi=0.014$ (0.058 Å) in (i), $\chi=0.010$ (0.056 Å) in (ii), and $\chi=0.008$ (0.050 Å) in (iii) directions. Although the shifts of oxygens were completely ignored in the present evaluations, it was known that the atomic shifts were almost the same as that in tetragonal $BaTiO_3$ (0.055 Å).[14] When we consider that the lattice distortion was small, the (iii) case accompanying the rhombohedral deformation seemed most probable. However, the final conclusion might be deferred.

B. Optical activity of ceramics

It is important to note that the presence of OA of ceramics cannot be determined solely by the symmetry of a constituent crystal but depends on the crystallite tex-

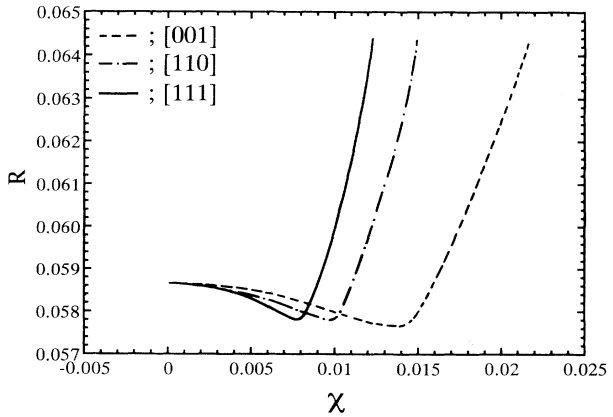

FIG. 6. Changes of R values with respect to fractional displacements χ of Ti and Zr atoms along [001], [110], and [111] directions.

ture of the ceramics. Therefore, it is necessary to deduce here the symmetry conditions for the presence of OA of the ceramics. In order to obtain the general rules, let us consider the ceramics composed of C_1 crystals, since they contain the most general properties of the least symmetries. The orientation of a crystal in the original (x_1,x_2,x_3) coordinate system is defined by a Eulerian angle (ω,θ,ψ) as depicted in Fig. 7, the coordinate system contained in the crystal being defined as (x_1''',x_2''',x_3'''). The two coordinates are related by the transformation matrix a_{ij},

$$\begin{bmatrix} x_1''' \\ x_2''' \\ x_3''' \end{bmatrix} = \begin{bmatrix} a_{11} & a_{12} & a_{13} \\ a_{21} & a_{22} & a_{23} \\ a_{31} & a_{32} & a_{33} \end{bmatrix} \begin{bmatrix} x_1 \\ x_2 \\ x_3 \end{bmatrix} , \tag{5}$$

where

$$a_{11}=\cos\psi\cos\omega\cos\theta-\sin\psi\sin\theta ,$$
$$a_{12}=\cos\psi\cos\omega\sin\theta+\sin\psi\cos\theta ,$$
$$a_{13}=-\cos\psi\sin\omega ,$$
$$a_{21}=-\sin\psi\cos\omega\cos\theta-\cos\psi\sin\theta ,$$
$$a_{22}=-\sin\psi\cos\omega\cos\theta+\cos\psi\cos\theta ,$$
$$a_{23}=\sin\psi\sin\omega ,$$
$$a_{31}=\sin\omega\cos\theta ,$$
$$a_{32}=\sin\omega\sin\theta ,$$

and

$$a_{33}=\cos\omega .$$

The gyration G, which will be observed along the beam direction $s'''(s_1''',s_2''',s_3''')$ is expressed as

$$G=\sum_{i,j} g_{ij}'''s_i'''s_j''' , \tag{6}$$

where g_{ij}''' are the gyration tensor components of the crystal. Then G can be also expressed in the original system by

$$G=\sum_{m,n} g_{mn}s_m s_n , \tag{7}$$

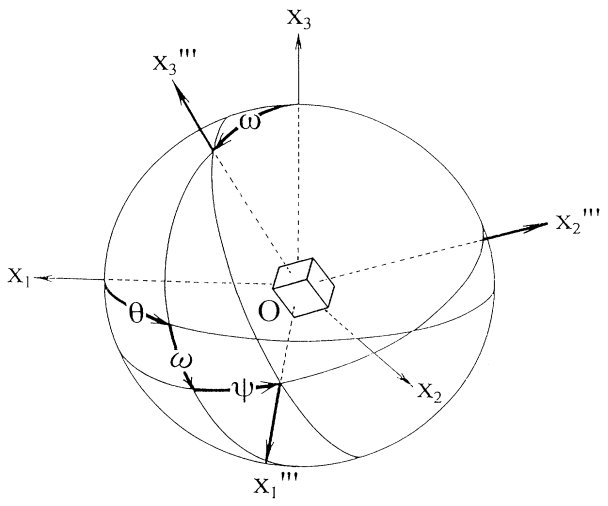

FIG. 7. Relationship between the original (x_1,x_2,x_3) coordinate system and (x_1''',x_2''',x_3''') coordinate system, which is rotated by Eulerian angles (θ,ω,ϕ).

where

$$g_{mm}=\sum_{i,j} g_{ij}'''a_{im}a_{jn} .$$

The gyration of the ceramics is expressed as

$$\bar{G}=\int_0^{\pi/2}\int_0^{2\pi}\int_0^{2\pi} G\sin\omega\alpha(\omega,\theta,\psi)d\omega\,d\theta\,d\psi . \tag{8}$$

Here $\alpha(\omega,\theta,\psi)$ is the density of crystallites located at the indicated Eulerian angles. It was evidenced from the present x-ray experiments that $\alpha(\omega,\theta,\psi)$ was a constant, defined M, in every θ, ω, and ψ position. From the orthogonal condition

$$M\int_0^{\pi/2}\int_0^{2\pi}\int_0^{2\pi}\sin\omega\,d\omega\,d\theta\,d\psi=1 , \tag{9}$$

M becomes $1/4\pi^2$. Then $\bar{G}$ reads

$$\bar{G}=\frac{1}{4\pi^2}\int_0^{\pi/2}\int_0^{2\pi}\int_0^{2\pi} G\sin\omega\,d\omega\,d\theta\,d\psi . \tag{10}$$

On the other hand, g_{mn} are expressed as follows:

$$\begin{aligned}
g_{11}=&(\cos^2\psi\cos^2\omega\cos^2\theta+\sin^2\psi\sin^2\theta-\tfrac{1}{2}\sin2\psi\sin2\theta\cos\omega)g_{11}''' \\
&+(\sin^2\psi\cos^2\omega\cos^2\theta+\cos^2\psi\sin^2\theta+\tfrac{1}{2}\sin2\psi\sin2\theta\cos\omega)g_{22}''' \\
&+\sin^2\omega\cos^2\theta g_{33}'''+\{\sin2\psi(\sin^2\theta-\cos^2\omega\cos^2\theta)-\cos2\psi\sin2\theta\cos\omega\}g_{12}''' \\
&+(\cos\psi\sin2\omega\cos^2\theta-\sin\psi\sin\omega\sin2\theta)g_{13}'''-(\sin\psi\sin2\omega\cos^2\theta+\cos\psi\sin\omega\sin2\theta)g_{23}''' , \\
g_{22}=&(\cos^2\psi\cos^2\omega\sin^2\theta+\sin^2\psi\cos^2\theta+\tfrac{1}{2}\sin2\psi\sin2\theta\cos\omega)g_{11}''' \\
&+(\sin^2\psi\cos^2\omega\sin^2\theta+\cos^2\psi\cos^2\theta-\tfrac{1}{2}\sin2\psi\sin2\theta\cos\omega)g_{22}''' \\
&+\sin^2\omega\sin^2\theta g_{33}'''+\{\sin2\psi(\cos^2\theta-\cos^2\omega\sin^2\theta)+\cos2\psi\sin2\theta\cos\omega\}g_{12}''' \\
&+(\cos\psi\sin2\omega\sin^2\theta+\sin\psi\sin\omega\sin2\theta)g_{13}'''-(\sin\psi\sin2\omega\sin^2\theta+\cos\psi\sin\omega\sin2\theta)g_{23}''' ,
\end{aligned}$$

$$
\begin{aligned}
g_{33} &= \cos^2\psi \sin^2\omega g'''_{11} + \sin^2\psi \sin^2\omega g'''_{22} + \cos^2\omega g'''_{33} - \sin 2\psi \sin^2\omega g'''_{12} - \sin 2\omega \cos\psi g'''_{13} + \sin\psi \sin 2\omega g'''_{23} , \\
g_{12} &= g_{21} = \tfrac{1}{2}(\cos^2\psi \cos^2\omega \sin 2\theta - \sin^2\psi \sin 2\theta + \sin 2\psi \cos 2\theta \cos\omega) g'''_{11} \\
&\quad + \tfrac{1}{2}(\sin^2\psi \cos^2\omega \sin 2\theta - \cos^2\psi \sin 2\theta - \sin 2\psi \cos 2\theta \cos\omega) g'''_{22} \\
&\quad + \tfrac{1}{2}\sin^2\omega \sin 2\theta g'''_{33} + \{\cos 2\psi \cos 2\theta \cos\omega - \tfrac{1}{2}\sin 2\psi (1 + \cos^2\omega) \sin 2\theta\} g'''_{12} \\
&\quad + (\sin\psi \cos 2\theta \sin\omega + \tfrac{1}{2}\cos\psi \sin 2\omega \sin 2\theta) g'''_{13} + (\cos\psi \cos 2\theta \sin\omega - \tfrac{1}{2}\sin\psi \sin 2\omega \sin 2\theta) g'''_{23} , \\
g_{13} &= g_{31} = \tfrac{1}{2}(-\cos^2\psi \sin 2\omega \cos\theta + \sin 2\psi \sin\theta \sin\omega) g'''_{11} \\
&\quad - \tfrac{1}{2}(\sin^2\psi \sin 2\omega \cos\theta + \sin 2\psi \sin\theta \sin\omega) g'''_{22} \\
&\quad + \tfrac{1}{2}\sin 2\omega \cos\theta g'''_{33} + \{\cos 2\psi \sin\theta \sin\omega + \tfrac{1}{2}\sin 2\psi \cos 2\omega \cos\theta\} g'''_{12} \\
&\quad + (\cos\psi \cos\theta \cos 2\omega - \sin\psi \cos\omega \sin\theta) g'''_{13} - (\sin\psi \cos\theta \sin 2\omega + \cos\psi \cos\omega \sin\theta) g'''_{23} ,
\end{aligned}
\tag{11}
$$

and

$$
\begin{aligned}
g_{23} &= g_{32} = -\tfrac{1}{2}(\cos^2\psi \sin 2\omega \sin\theta + \sin 2\psi \cos\theta \sin\omega) g'''_{11} \\
&\quad + \tfrac{1}{2}(-\sin^2\psi \sin 2\omega \sin\theta + \sin 2\psi \cos\theta \sin\omega) g'''_{22} \\
&\quad + \tfrac{1}{2}\sin 2\omega \sin\theta g'''_{33} + \{-\cos 2\psi \cos\theta \sin\omega + \tfrac{1}{2}\sin 2\psi \sin 2\omega \sin\theta\} g'''_{12} \\
&\quad + (\cos\psi \sin\theta \cos 2\omega + \sin\psi \cos\omega \cos\theta) g'''_{13} + (-\sin\psi \sin\theta \cos 2\omega + \cos\psi \cos\omega \cos\theta) g'''_{23} .
\end{aligned}
$$

When G is substituted into (10), $\bar{G}$ becomes

$$\bar{G} = \tfrac{1}{3}(g'''_{11} + g'''_{22} + g'''_{33})(s_1^2 + s_2^2 + s_3^2) . \tag{12}$$

If $\bar{g}_{mn}$ is defined as a gyration tensor component of the ceramics,

$$\bar{G} = \sum_{m,n} \bar{g}_{mn} s_m s_n . \tag{13}$$

$\bar{g}_{mn}$ derived from g'''_{ij} of the 15 optically active classes are classified in Table II, where the triple primes are omitted. An important conclusion can be drawn from the table that the ceramics composed homogeneously of optically active nonenantiomorphic classes become optically inactive.

TABLE II. Gyration tensors $\bar{g}_{mn}$ of 15 optically active classes in ceramic states.

Point group	Gyration tensor
C_1, C_2, D_2	$\begin{bmatrix} \frac{g_{11}+g_{22}+g_{33}}{3} & \cdot & \cdot \\ \cdot & \frac{g_{11}+g_{22}+g_{33}}{3} & \cdot \\ \cdot & \cdot & \frac{g_{11}+g_{22}+g_{33}}{3} \end{bmatrix}$
$C_3, C_4, C_6,$ D_3, D_4, D_6	$\begin{bmatrix} \frac{2g_{11}+g_{33}}{3} & \cdot & \cdot \\ \cdot & \frac{2g_{11}+g_{33}}{3} & \cdot \\ \cdot & \cdot & \frac{2g_{11}+g_{33}}{3} \end{bmatrix}$
O, T	$\begin{bmatrix} g_{11} & \cdot & \cdot \\ \cdot & g_{11} & \cdot \\ \cdot & \cdot & g_{11} \end{bmatrix}$
C_s, C_{2v}, S_4, D_{2d}	$\begin{bmatrix} \cdot & \cdot & \cdot \\ \cdot & \cdot & \cdot \\ \cdot & \cdot & \cdot \end{bmatrix}$

C. Determination of crystal classes of high- and low-temperature phases

We tried to determine group theoretically the crystal classes of the H and L phases which are consistent with the HAUP results expressed in Fig. 4. The characteristic optical features of the H and L phases observed by the HAUP method are summarized in Table III.

The L phase is ferroelectric and undoubtedly optically active. The classes which permit both conditions are limited to C_1, C_2, C_3, C_4, C_6, C_s, and C_{2v}. Among these classes the last two should be excluded from the candidates of the L phase by a reason referring to Table II. The optical conditions for a class to be an H phase are as follows: (i) It is optically inactive. (ii) It does not show electrogyration effects. (iii) It contains ferroelectric groups C_1, or C_2, or C_3, or C_4, or C_6, as its subgroups. Among five classes in the cubic system, O_h, T_d, and T_h satisfy condition (i), while O and T must be excluded from the candidates of the H phase. Of course, O_h satisfies (ii), but it must be noted that T_d and T_h do also. In T_d, there exist second-order electrogyration coefficients $\nu_{13}=-\nu_{23}$. Therefore $g_{11}=-g_{22}$ will appear by the application of E_3. However, these coefficients are equivalent to an off-diagonal component g_{12}, which vanishes in the ceramic state. The same reasoning can be applied to T_h ceramics, where g_{12} appearing through μ_{63} vanishes in the state. Thus T_d and T_h can also be candidates of the H phase at this stage.

A polarization vector $\mathbf{P}(P_x,P_y,P_z)$ can be the bases of the vector irreducible representations, e.g., T_u representation in T_h, of the five cubic classes. Here the following conditions are applied to the components of $\mathbf{P}$: (1) $P_x\neq 0, P_y=P_z=0$, and their cyclic equivalent components; (2) $P_x=P_y\neq 0$, $P_z=0$; (3) $P_x\neq P_y\neq 0$, $P_z=0$; (4) $P_x=P_y=P_z\neq 0$; (5) $P_x=P_y\neq P_z\neq 0$; and (6) $P_x\neq P_y\neq P_z\neq 0$. Then each vector stays invariant by the operations of some component symmetry elements contained in any class. For example, vector (1) in the basis of T_u irreducible representation of T_h becomes invariant by the following representations:

$$\begin{matrix} E & & & C_{2x} & & & \sigma_y & & & \sigma_z & \\ \begin{bmatrix} 1 & \cdot & \cdot \\ & 1 & \cdot \\ & & 1 \end{bmatrix}, & \begin{bmatrix} 1 & \cdot & \cdot \\ & -1 & \cdot \\ & & -1 \end{bmatrix}, & \begin{bmatrix} 1 & \cdot & \cdot \\ & -1 & \cdot \\ & & 1 \end{bmatrix}, & \begin{bmatrix} 1 & \cdot & \cdot \\ & 1 & \cdot \\ & & -1 \end{bmatrix}. \end{matrix} \tag{14}$$

TABLE III. Characteristic optical features of H and L phases.

	Optical activity		Birefringence	
Phase	Spontaneous gyration	Electrogyration effect	Spontaneous birefringence	Electrooptic effect
H	None	None	None	Yes (quadratic)
L	Yes	Yes (butterfly hysteresis)	Yes	Yes (butterfly hysteresis)

These symmetry elements constitute a ferroelectric subgroup C_{2v}. In Table IV, six ferroelectric subgroups of T_h are tabulated for six polarizations (1)–(6). In this way, all the ferroelectric subgroups of the five cubic classes are tabulated in Table V, where the subgroups, which can be optically active in the ceramic states, are shaded.

From Table V, the following facts can be obtained: (1) C_1 is the subgroup of all the classes. (2) C_2 is the subgroup of T and O. However, T and O cannot be an H phase as mentioned above. Accordingly, C_2 cannot be a class of L phase. (3) C_3 is the subgroup of O, T_h and T. However O and T cannot be the class of H phase. Therefore it is connected only with T_h as its subgroup. (4) C_4 is a subgroup only of O. Therefore it cannot be a class of L phase. (5) C_6 cannot be a subgroup of all the classes. Thus H phase can be transformed into ferroelectric L phases only through the following paths; $O_h\rightarrow C_1, T_h\rightarrow C_1$ and C_3, and $T_d\rightarrow C_1$. Judging from the previous x-ray examinations, C_1 could not be a class of L phase. Thus it was uniquely determined that the point groups of H and L phase were cubic T_h and trigonal C_3, respectively. They can be transformed into each other with the second order. This fact coincides with the x-ray evidence that C_3 is the most probable class of L phase. It is surprising that the prototype class of PLZT is different from that of $PbTiO_3$ and $PbZrO_3$. However, the information of the optical activity of both phases definitely led us to make this conclusion.

IV. PHASE TRANSITION OF PLZT

As the classes of H and L temperature phases were determined, we reached a position where the transition mechanism could be elucidated. As the first step, it was necessary to clarify the relation which connects the polarization reversal with the crystallographic twinning mechanisms under the consistent conditions of the symmetry change between the T_h and C_3 phases.

The electrooptic effects in C_3 are realized through the linear and quadratic electrooptic coefficients s_{ij} and r_{ij} of the T_h phase, which are indicated in Fig. 8(a). There exist no components in s_{ij} and four components in r_{ij}; r_{11}, r_{12}, r_{21}, and r_{44}. Two kinds of twinning operations accompanied by polarization reversal are indicated in Table VI. When the four components of r_{ij} are transformed by the rotation twinning operation, the resulting coefficients r_{ij}^* are expressed;

$$r_{11}^*=r_{11},\quad r_{12}^*=r_{12},\quad r_{21}^*=r_{21},\quad \text{and } r_{44}^*=r_{44}\ . \tag{15}$$

Therefore the composite electro-optic coefficient r of the T_h ceramics will be transformed into r^* by the same operation, when

$$r^*=r\ . \tag{16}$$

Then the birefringences Δn and Δn^* of the ceramics before and after a polarization reversal are related:

$$\Delta n=\Delta n^*=r(P_s+P)^2\doteqdot rP_s^2+2rP_sP\ . \tag{17}$$

Δn^* and Δn are unaltered by the change of the sign of P, and a butterfly hysteresis will be formed. As were al-

TABLE IV. Bases, invariant representations, and subgroups of a vector representation of T_h.

Basis	Invariant representation				Subgroup
$P_x\neq0,\ P_y=P_z=0$	E $\begin{bmatrix}1&&\\&1&\\&&1\end{bmatrix}$	C_{2x} $\begin{bmatrix}1&&\\&-1&\\&&-1\end{bmatrix}$	σ_y $\begin{bmatrix}1&&\\&-1&\\&&1\end{bmatrix}$	σ_z $\begin{bmatrix}1&&\\&1&\\&&-1\end{bmatrix}$	C_{2v}
$P_x=P_y\neq0,\ P_z=0$	E $\begin{bmatrix}1&&\\&1&\\&&1\end{bmatrix}$	σ_z $\begin{bmatrix}1&&\\&1&\\&&-1\end{bmatrix}$			C_s
$P_x\neq P_y\neq0,\ P_z=0$	E $\begin{bmatrix}1&&\\&1&\\&&1\end{bmatrix}$	σ_z $\begin{bmatrix}1&&\\&1&\\&&-1\end{bmatrix}$			C_s
$P_x=P_y=P_z\neq0$	E $\begin{bmatrix}1&&\\&1&\\&&1\end{bmatrix}$	$C^+_{3[111]}$ $\begin{bmatrix}&&1\\1&&\\&1&\end{bmatrix}$	$C^-_{3[111]}$ $\begin{bmatrix}&1&\\&&1\\1&&\end{bmatrix}$		C_3
$P_x=P_y\neq P_z\neq0$	E $\begin{bmatrix}1&&\\&1&\\&&1\end{bmatrix}$				C_1
$P_x\neq P_y\neq P_z\neq0$	E $\begin{bmatrix}1&&\\&1&\\&&1\end{bmatrix}$				C_1

ready described, this phenomenon accorded with the experimental facts. It is seen by the analogous process that (15) holds when the reflection twinning operation is applied, and accordingly (17) also holds. Thus the change of Δn accompanied by a polarization reversal will be always shown in the form of a butterfly hysteresis. This means that the experimental results on the change of Δn are consistent with any of the twinning mechanisms.

Electrogyration coefficients of the C_3 phase are indicated in Fig. 8(b). The OA of the C_3 phase takes place through the linear and quadratic electrogyration coefficients, μ_{ij} and ν_{ij}. We calculated the gyration G of ceramics of C_3 crystals:

$$G=\tfrac{1}{3}\{(2\mu_{13}+\mu_{33})P_s+(2\nu_{13}+\nu_{33})P_s^2\}+\tfrac{1}{8}\{3\mu_{13}+\mu_{33}-2\mu_{51}+2(3\nu_{13}+\nu_{33}-\nu_{44})P_s\}P\ . \tag{18}$$

The calculation of G was made under the same spirit of deduction of (11), and the detailed processes are omitted here. In the case of a rotation twinning operation,

$$\mu^*_{13}=-\mu_{13},\quad \mu^*_{33}=-\mu_{33},\quad \mu^*_{51}=-\mu_{51}$$

and (19)

$$\nu^*_{13}=\nu_{13},\quad \nu^*_{33}=\nu_{33},\quad \nu^*_{44}=\nu_{44}\ .$$

TABLE V. Possible ferroelectric subgroups of all the cubic classes.

Basis \ Class	O_h	T_d	O	T_h	T
$P_x\neq0,\ P_y=P_z=0$	C_{4v}	C_{2v}	C_4	C_{2v}	C_2
$P_x=P_y\neq0,\ P_z=0$	C_{2v}	C_s	C_2	C_s	C_1
$P_x\neq P_y\neq0,\ P_z=0$	C_s	C_1	C_1	C_s	C_1
$P_x=P_y=P_z\neq0$	C_{3v}	C_{3v}	C_3	C_3	C_3
$P_x=P_y\neq P_z\neq0$	C_s	C_s	C_1	C_1	C_1
$P_x\neq P_y\neq P_z\neq0$	C_1	C_1	C_1	C_1	C_1

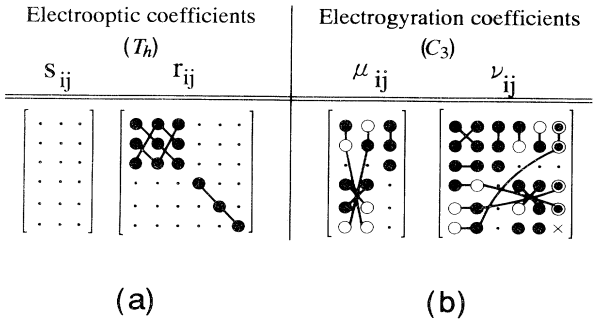

FIG. 8. Electrooptic coefficients of T_h (a), and electrogyration coefficients of C_3 (b).

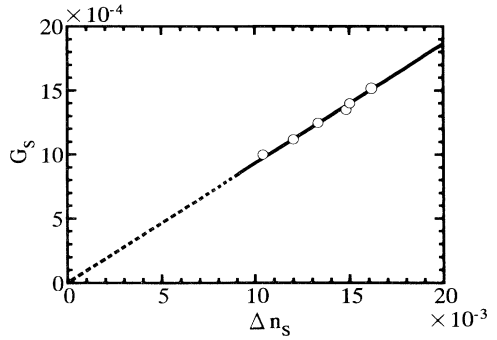

FIG. 9. Relation of G_s with respect to Δn_s of PLZT (8/70/30) in the L phase.

Therefore

$$G^* = G \ . \tag{20}$$

A butterfly hysteresis will be formed by a polarization reversal. In the case of reflection twinning operation, the opposite changes of μ_{ij} and ν_{ij} will occur to (19). Therefore

$$G^* = -G \ . \tag{21}$$

In this case, a square hysteresis will be formed. As the experimental hystereses were undoubtedly of the butterfly type, it was determined that a polarization reversal in the C_3 phase takes place through the formation of the rotation twins. Then the spontaneous gyration G_s is expressed as

$$G_s = \mu P_s + \nu P_s^2 \ , \tag{22}$$

where $\mu = 1/3(2\mu_{13} + \mu_{33})$, and $\nu = 1/3(2\nu_{13} + \nu_{33})$. On the other hand, the spontaneous birefringence Δn_s is written from (17):

$$\Delta n_s = r P_s^2 \ . \tag{23}$$

The observed G_s were found to be strictly in a linear relation with respect to the observed Δn_s as depicted in Fig. 9. It indicated that G_s depends exclusively on P_s^2 as the result of the vanishing of μ.

Judging from E dependences of Δn and G in a temperature range between 15 and 20 °C, it seemed very likely that a second-order phase transition, which was apparently modified to a first-order one, took place around these temperature regions (defined as a "transition region" in what follows). On the other hand, it is necessary at this stage to quote briefly previous reports on dielectric properties of PLZT(8/65/35). In Fig. 10, the temperature dependence of ε,[1,2] remanent polarization P_r,[1,2] and P-E hysteresis loops[1] are indicated. There is a broad maximum of ε at T_m. P_r does not vanish at a definite characteristic temperature, so-called slim hysteresis loops existing even above T_m. Looking at the previous evidence, it seemed to us that the dielectric properties of PLZT would be too difficult to be explained by a single mechanism which could account for the results of the HAUP measurements in the vicinity of the transition region. We tried to elucidate the phase transition of PLZT in the following ways: to determine exactly the potential function of the T_h phase which drives it to transform into the C_3 phase, and to extract anomalous parts of dielectric properties perturbed from the expected properties of the potential function.

TABLE VI. Transformation matrices of twinning operations.

Rotation twinning	Reflection twinning
$\begin{bmatrix} 1 & 0 & 0 \\ 0 & \bar{1} & 0 \\ 0 & 0 & \bar{1} \end{bmatrix}$	$\begin{bmatrix} 1 & 0 & 0 \\ 0 & 1 & 0 \\ 0 & 0 & \bar{1} \end{bmatrix}$

Let us develop a phenomenological theory of the second-order phase transition between the T_h and C_3 phases. A potential function of the T_h phase can be written, taking polarization P along the [111] direction as an order parameter:

$$A = A_0 + \frac{1}{2}\frac{T - T_0}{C}P^2 + \frac{1}{4}\gamma P^4 + \frac{1}{6}\delta P^6 \ , \tag{24}$$

where C represents the Curie constant, and T_0 the critical temperature. On the other hand, from (17) Δn is expressed,

$$\Delta n = r^E E^2 = r^P P^2 \ , \tag{25}$$

where r^E and r^P are electro-optic coefficients of ceramics referring to E and P. Both coefficients are related with each other;

$$r^E = (\varepsilon_0 \varepsilon_+)^2 r^P = \frac{C^2 r^P}{(T - T_0)^2} \ , \tag{26}$$

where ε_+ represents the dielectric constant in the high-temperature branch, ε_0 the dielectric constant of the vacuum. r^E were determined at various temperatures between 20 and 90 °C such that observed Δn values were fitted with a function of E^2. $1/\sqrt{r^E}$ thus obtained are plotted against T in Fig. 11. It changes linearly in the lower-temperature side and crossed with the abscissa at $T_0 = -16$ °C, below which only a ferroelectric state is stable. However, the linear relation breaks rather sud-

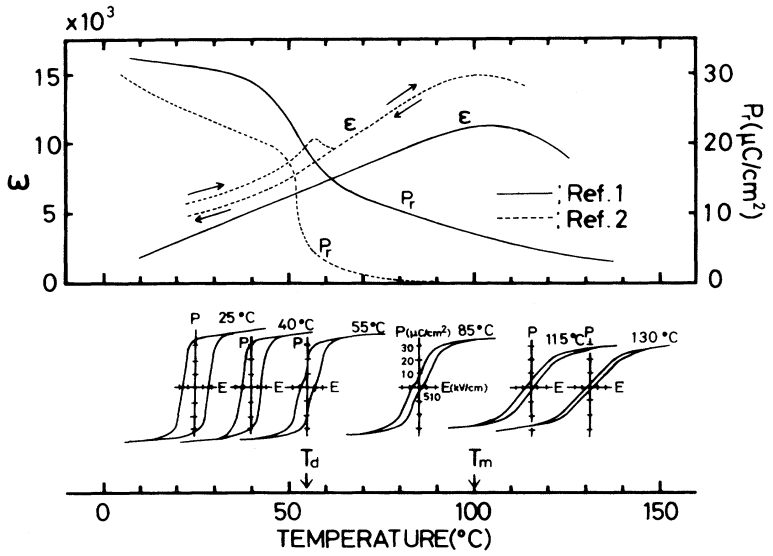

FIG. 10. Temperature dependence of ε, remanent polarization P_r, and P-E hysteresis loops (previous reports).

denly above 70 °C. From the derivative of the line,

$$C\sqrt{r^P}=3.98\times10^{-6}\ (\mathrm{K\,m/V})\ . \tag{27}$$

On the other hand, the dielectric stiffness $1/\varepsilon_-$ in the low-temperature branch is given:

$$\frac{1}{\varepsilon_-}=-4\frac{T-T_0}{C}+\frac{\gamma^2}{\delta}\{1+\sqrt{1-(4\delta/\gamma^2C)(T-T_0)}\}\ . \tag{28}$$

Therefore it becomes zero at

$$T_1=T_0+\frac{1}{4}\frac{\gamma^2C}{\delta}\ , \tag{29}$$

above which the ferroelectric state can exist only under electric fields. In the C_3 phase, the derivative $|s^E|$ of Δn with respect to E at $E=0$ is expressed as

$$|s^E|=\left|\frac{d\Delta n}{dE}\right|_{E=0}=2\varepsilon_0\varepsilon_-r^PP_s\ . \tag{30}$$

Accordingly $1/|s^E|$, which must be proportional to $1/\varepsilon_-$, should become zero at T_1. Observed values of $1/|s^E|$ were plotted against T in Fig. 12; T_1 was determined to be 19 °C. Therefore, from (29), $\gamma^2C/\delta=140$ K. P_s^2 can be deduced from (24) by using a condition of $E=\partial A/\partial P=0$,

$$P_s^2=-\frac{\gamma}{2\delta}\{1+\sqrt{1-(4\delta/\gamma^2C)(T-T_0)}\}\ . \tag{31}$$

By substituting it into (25), spontaneous birefringence Δn_s was given:

$$\Delta n_s=-\frac{\gamma r^P}{2\delta}+\sqrt{(-\gamma r^P/2\delta)^2-[(r^P)^2/C\delta](T-T_0)}\ . \tag{32}$$

$-\gamma r^P/2\delta$ and $(r^P)^2/C\delta$, which were fitted with the temperature dependence of Δn_s, were determined to be 1.63×10^{-2}, and 1.90×10^{-6} K, respectively. In Fig. 13, the calculated Δn_s (solid line) are compared with the observed Δn_s (circles).

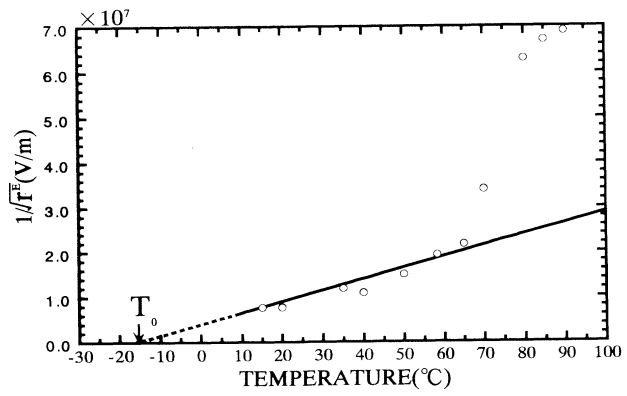

FIG. 11. Temperature dependence of $1/\sqrt{r^E}$ of PLZT(8/70/30).

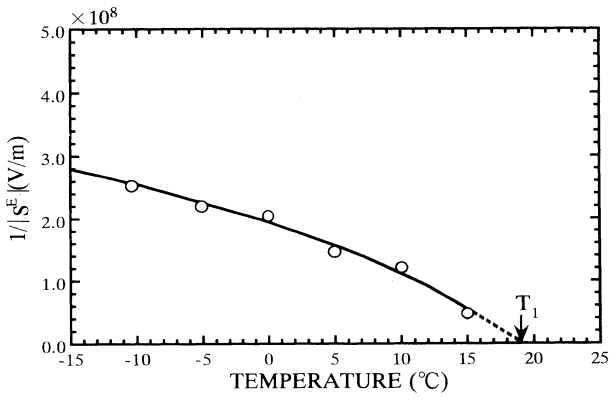

FIG. 12. Temperature dependence of $1/|s^E|$ of PLZT(8/70/30).

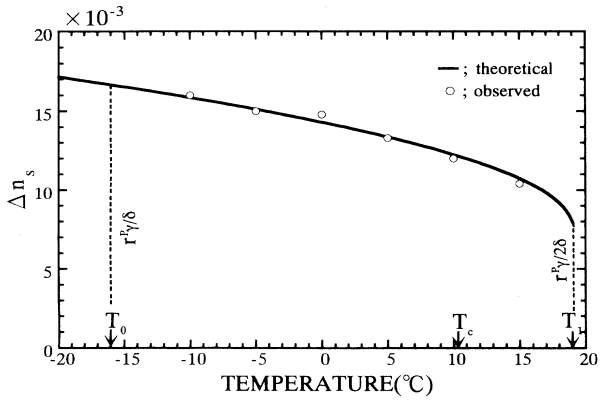

FIG. 13. Comparison of temperature dependences of calculated and observed Δn_s in the L phase.

Summarizing the above results, principal coefficients were obtained as follows: $r^P=15.84\times10^{-2}/C^2$, $\gamma=-1.36\times10^{-7}/C^3$, and $\delta=1.32\times10^{-16}/C^5$. In order to obtain the absolute values of the above coefficients C might be determined. However, this was a difficult problem. Measured ε in the vicinity of the transition region would not represent perfectly the purely characteristic fluctuation associated with the phase transition, since it would be smeared by the anomalous fluctuation of the perturbed state to a considerable extent. In a sufficiently higher-temperature region, the anomalous fluctuation will decay, but instead the critical state characteristic of the transition will disappear.

ε were measured by using a LCR meter on a specimen with area of $604\times612\ \mu m^2$ and thickness of 82 μm. Temperature dependences of ε with frequencies of 0.12, 1, and 10 kHz are depicted in Fig. 14. They manifested the characteristic nature of a relaxor of the specimen; the maxima of ε shift to the higher-temperature side very slightly by increase of frequencies. Solid circles indicated above 0 °C represent the result at 0.12 kHz in the heating process of the specimen, which was poled beforehand at 0 °C by a biasing field of 4 kV/cm for 3 h. A sharp peak appeared in this case at 19 °C, which could not be found in the cooling process of an unbiased condition. The relation between $1/\varepsilon$ and T is shown in Fig. 15. It is known thermodynamically that $1/\varepsilon_+$ becomes zero at T_0, which was already determined. The problem was, then, to determine the derivative of the straight line of $1/\varepsilon_+$ in the higher-temperature region. The most plausible line was drawn in the figure such that it begins from T_0 and coincides with observed stiffness at a high-temperature region; thus we determined, $C=4.4\times10^{-6}$ K F/m. Then the thermodynamical constants were determined as shown in Table VII, where the corresponding values of $BaTiO_3$ (Ref. 15) are also shown for the sake of comparison. Here T_c is the transition temperature, and T_2 is the maximum temperature where the ferroelectric state can exist under applied E. It turned out that the thermodynamical constants differ considerably between the two crystals.

By using the above values, theoretical relations of P vs E, Δn vs E, and G vs E were evaluated and compared with the experimental results in Figs. 16 and 17. Figures $16(a_1)-16(a_3)$ represent these relations at a temperature of 0 °C, between T_0 and T_c. In Figs. $16(a_2)$ and $16(a_3)$, the agreement of experimental and theoretical values was excellent when the difficult experimental conditions are taken into account. In Figs. $16(b_1)-16(b_3)$, which indicate the relations at 10 °C, just below T_c, the agreement was still good. In Fig. $16(c_2)$, the relation at 15 °C, above of T_c, the agreement of Δn is good when $|E|$ decreased from both sides. However, the transitions of Δn from low-value to high-value branches delayed from the theoretical curves. In Fig.$16(c_3)$, the observed G decreased more quickly than the theoretical curves when $|E|$ were decreased. In Fig. $16(d_2)$, at 20 °C, approximately T_1, Δn dropped to the low-value branch earlier than the theoretical curves, and retarded in reaching the high-value branches. The same was the case for G in Fig.

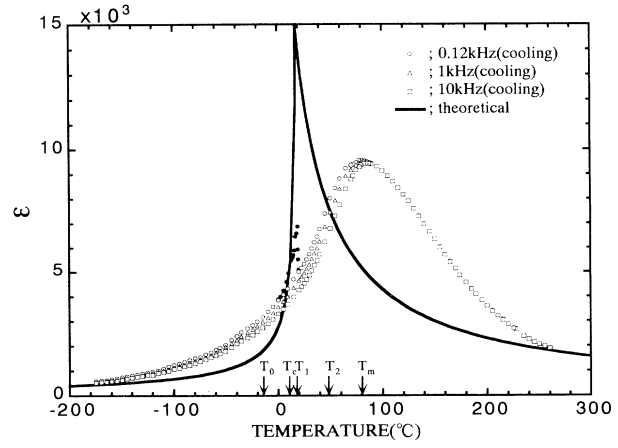

FIG. 14. Temperature dependence of ε measured with frequencies of 0.12, 1, and 10 kHz. Theoretical values of ε are drawn by the solid lines.

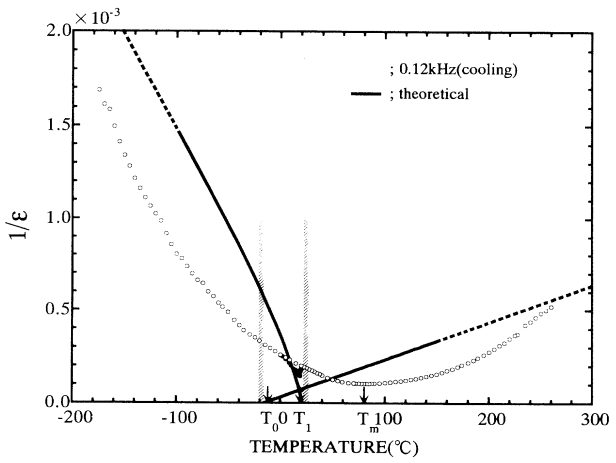

FIG. 15. Temperature dependence of $1/\varepsilon$ of 0.12 kHz. The solid lines indicate the theoretical values.

TABLE VII. Thermodyanamical coefficients and transition temperatures of PLZT and $BaTiO_3$.

	PLZT(8/70/30)	$BaTiO_3$ (Ref. 15)
C (K F/m)	4.4×10^{-6}	1.1×10^{-6}
C/ε_0 (K)	5.0×10^{5}	1.3×10^{5}
γ (m^5 V/C^3)	-1.6×10^{9}	-3.5×10^{9}
δ (m^9 V/C^5)	8.0×10^{10}	2.7×10^{11}
r^P (m^4/C^2)	8.2×10^{-1}	
T_0 (°C)	−16.0	118.0
T_c-T_0 (°C)	26.3	7.7
T_1-T_0 (°C)	35.0	10
T_2-T_0 (°C)	63.2	18

TABLE VIII. Optical rotatory powers of crystals.

Substance	λ (Å)	T (°C)	ρ (°/mm)	Ref.
α-$AlPO_4$	6328		−14.6	17
$AgGaS_2$	4850		950.0	18
$Ca_2Sr(C_2H_5COO)_6$	5890	20	4.2	19
α-HgS	6328		−320.0	20
$Bi_{12}SiO_2$	6500		−20.5	21
α-$LiIO_3$	6328		−86.7	22
$[N(CH_3)_4]_2ZnCl_4$	6328	21	0.05	9
α-SiO_2	6328	20	25.1	10
TeO_2	6328		87.0	23
Hg_2I_2	6328		232.0	23
$[N(CH_3)_4]_2CuCl_4$	6328	24	7.6	24
$NaKC_4H_4O_6\cdot4H_2O$	6328	25	−0.96	25
$BaMnF_4$	6328	−140	5.7	26
$(C_3H_7NH_3)_2MnCl_4$	6328	82	2.2	27
$(NH_2CH_2CO_2H)_3H_2SO_4$	6328	32	1.9	28
$LiNH_4C_4H_4O_6\cdot H_2O$	6328	−190	−3.9	29
PLZT(8/70/30) (ceramics)	6328	15	102	Present work

16(d_3). In Fig. 17(a_2), at 35 °C, between T_1 and T_2, it became rather sudden that the high-field values of Δn were conspicuously lowered from the theoretical curves and the deformed hysteresis loops shifted to high fields sides. Besides, in Fig. 17(a_3), the departure of the observed G from the theoretical curves became more remarkable than in Δn. In Figs. 17(b_2), and 17(b_3), at 40 °C, below T_2, the discrepancies of Δn and G became larger. In Fig. 17(c_2), at 50 °C, just above T_2, the hysteresis loops of Δn coalesced into linear changes. G took place slightly only in high field sides. In Fig. 17(d_2), at 80 °C, the induction of Δn was too small to be expressed in this figure, although the theoretical values still stayed at considerable values. G does not appear at all within the indicated E.

From the comparison of observed and theoretical behaviors of Δn and G at various temperatures it has become evident that Δn and G change according very closely to the theoretical predictions in the transition region, but begin to deflect from them at about T_1, and the deviations become serious above T_2. Above 80 °C, G disappears and even Δn fades away to lower orders of magnitude.

The theoretical ε calculated by using the thermodynamical constants are indicated in Fig. 14 by solid lines, and compared with the observed ones, where the characteristic temperatures are indicated in the abscissa. It must be noted that both kinds of curves almost coincide above 300 °C and below −160 °C. However, the

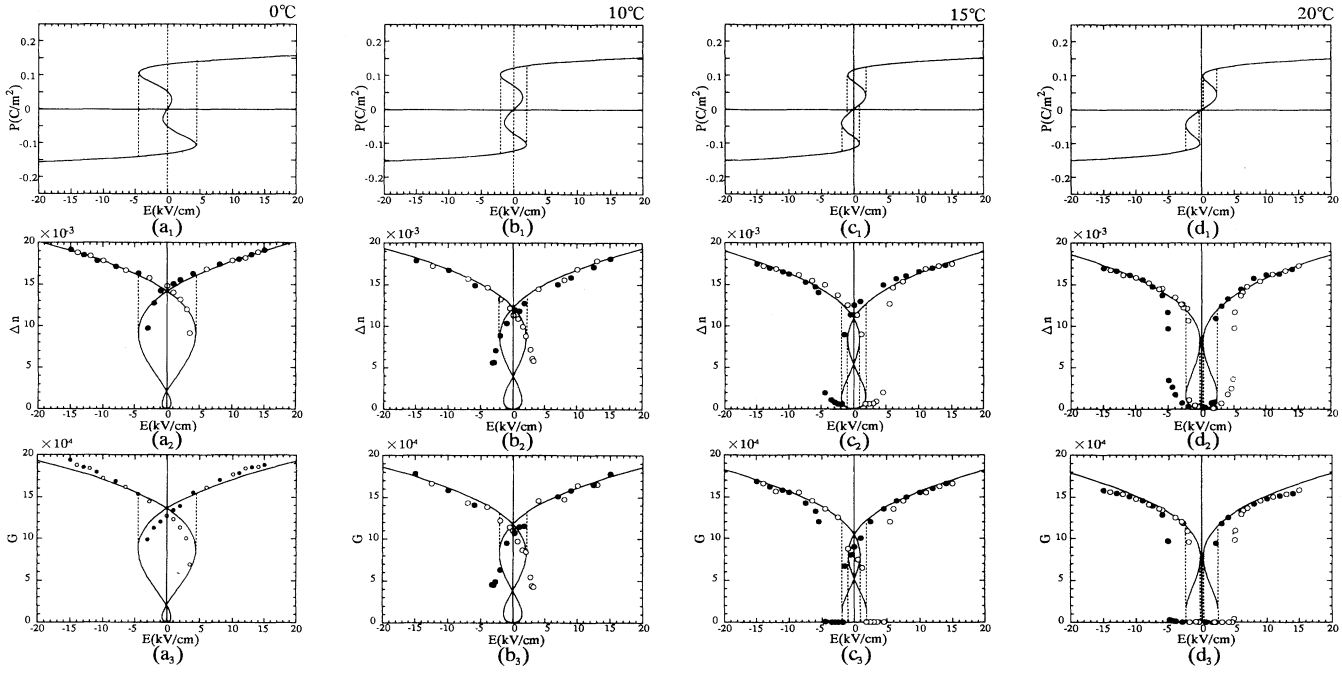

FIG. 16. Comparisons of theoretical relations of P vs E, Δn vs E, and G vs E with observed ones. (a) 0 °C; (b) 10 °C; (c) 15 °C; and (d) 20 °C.

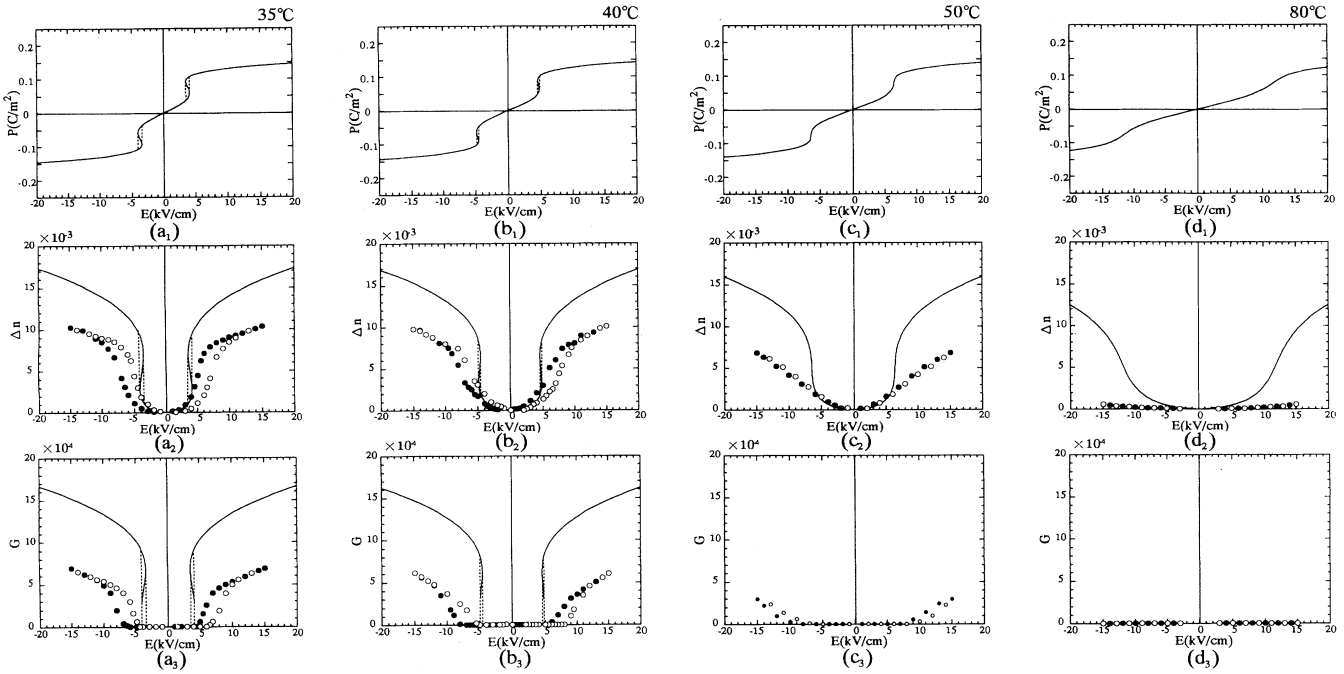

FIG. 17. Comparisons of theoretical relations of P vs E, Δn vs E, and G vs E with observed ones. (a) 35 °C; (b) 40 °C; (c) 50 °C; and (d) 80 °C.

disagreement within this temperature interval is conspicuous. It is of particular interest that a small peak of solid circles, which are mentioned before, just lies on the theoretical line around T_c. This phenomenon may be related to an aging effect of PLZT, which was reported by Schulze, Biggers, and Cross.[16] It confirms that the dielectric property of PLZT is predominantly controlled by the second-order phase transition in a narrow temperature interval between T_0 and T_1. $1/\varepsilon$ of both branches are also compared in Fig. 15. The figure suggests a picture for interpreting the dielectric property of PLZT. In the shaded temperature region in the figure, observed and theoretical E dependences of Δn and G were coincided. This figure definitely reveals that the occurrence of the second-order phase transition at $T_c = 10.3$ °C is the fundamental basis of the dielectric property of PLZT. Besides, unusually large fluctuation takes place in the wider temperature region. It is also of interest that the physical meaning of T_m becomes unambiguous at this stage. It is nothing else but the minimum point of $1/\varepsilon$ connecting broadly its H temperature and L temperature branches.

V. CONCLUSIONS AND DISCUSSIONS

As the results of the HAUP study on Δn and G, the occurrence of a second-order phase transition between the T_h and C_3 phases has been clearly revealed. The transition was further confirmed by using x-ray diffractions. Nevertheless, it was also clarified that physics of PLZT becomes suddenly difficult to be understood as the temperature departs from the shaded region in Fig. 15. Rather it may be said that the complexity of PLZT has become more definitive by the present study. Therefore, it would be important at this stage to clarify what has been revealed and what has been left ambiguous.

The evidences obtained in the present study are summarized in the following. (1) The H and L temperature phases are cubic T_h and trigonal C_3, respectively. The second-order phase transition between the phases is changed apparently into the first-order one due to the presence of the negative coefficient of P^4 terms in the free energy. The free-energy function was determined by finding the relevant coefficients as tabulated in Table VII.

TABLE IX. Electrogyration coefficients of crystals.

Substance	Electrogyration coefficient (m^4/C^2)	Ref.
$NaKC_4H_4O_6 \cdot 4H_2O$	$\lvert\nu_{11}\rvert = 2.80$	25
α-SiO_2	$\lvert\nu_{11}\rvert = 3.99 \times 10^3$	30
$[N(CH_3)_4]_2ZnCl_4$	$\lvert\nu_{13}\rvert = 1.90 \times 10$	31
$Ca_2Sr(C_2H_5COO)_6$	$\lvert\nu_{13}\rvert = 1.60 \times 10^3$	32
$Co_3B_7O_{13}I$	$\lvert\nu_{13}\rvert = 1.60 \times 10^4$	33
PLZT(8/70/30) (ceramics)	$\nu^P = 7.10 \times 10^{-2}$	Present work

TABLE X. Linear electro-optic coefficients of crystals.

Substance	λ (Å)	T (°C)	ε_- (F/m)	s^E (10^{-10} m/V)	s^P (m^2/C)	Ref.
$LiNbO_3$	6328	20	32	1.12	0.41	34
$LiTaO_3$	6328	20	45	1.14	0.29	35
$BaTiO_3$	6328	25	135	1.25	0.11	36
PLZT(8/40/60) (ceramics)	6328	15	600	8.0	0.15	1
PLZT(8/65/35) (ceramics)	6328	15	2000	48	0.27	1
PLZT(8/70/30) (ceramics)	6328	0	3600	55	0.17	Present work

The coefficients differ considerably from those of $BaTiO_3$.[15] (2) As the polarized phase belongs to the trigonal system the lattice strains are less conspicuous than those of other perovskite ferroelectrics. Atomic shifts of Ti and Zr atoms are approximately 0.050 Å, the same order of magnitude of Ti in tetragonal $BaTiO_3$.[15] (3) Optical rotatory power ρ of PLZT is approximately 102°/mm, very large compared with other crystals as can be seen in Table VIII. The electrogyration coefficient is about 7.07×10^{-2} m^4/C^2, very small as can be seen in Table IX. The electro-optic coefficient s^E evaluated from the Δn vs E relation at 0 °C [Fig. 16(a_2)] is 55×10^{-10} m/V. It is compared with other crystals in Table X.

Phenomena which cannot be explained within the present framework of the thermodynamical model are summarized: (1) Deviations of the electro-optic and electrogyration effects from those predicted from the free-energy function begin to occur around T_1 and become conspicuous with an increase of temperature. (2) Discrepancy of the observed and theoretical $1/\varepsilon$ is remarkable as can be seen in Fig. 15. (3) G_s does not disappear sharply above $T_2=47.2$ °C, and the C_3 phase does not always take place below $T_0=-16$ °C when biasing E are not applied.

Finally we feel it a task to mention briefly our idea on these puzzling problems. It must be emphasized again that an anomalously large fluctuation takes place in PLZT at a wider temperature range as can be seen in Fig. 15. This phenomenon will have close bearing on the mechanism of the building up of macrodomains and decay back to disorder microdomains. When macrodomains have been built up regularly from the microdomains it should manifest the free-energy-controlled dielectric properties. When they decay to disordered microdomains the free-energy-controlled property will fade away. On the other hand, the affinity to the disordered state is dependent on temperature, increasing as temperature deviates from T_c. For instance, in Fig. 17(d_2), Δn appeared very slightly up to 15 kV/cm. However, it may be that Δn could become the free-energy-controlled values when sufficiently large E is applied. At higher temperature above about 300 °C, this mechanism diminishes and PLZT will become a normal dielectric. On the other hand, an increase of fluctuation will elongate the relaxation time for building up the macrodomains by the application of E. The formation of slim hysteresis loops, and appearance of P_r at higher temperatures than T_1, may be due to this effect. On the other hand, the HAUP experiments were performed under quasistatic conditions. This could be the reason why the spontaneous Δn markedly differ from prescribed values by P_r. HAUP experiments on specimens with wider concentrations will be necessary for further resolution of the dielectric property of PLZT.

ACKNOWLEDGMENTS

This work was supported by Research Development Corporation of Japan. The authors thank I. Kamiya, H. Utsumi, and M. Nakamura for their contributions to the measurements of dielectric constants.

[1]G. H. Haertling and C. E. Land, J. Am. Ceram. Soc. **54**, 1 (1971).
[2]E. T. Keve and A. D. Annis, Ferroelectrics **5**, 77 (1973).
[3]E. T. Keve and K. L. Bye, J. Appl. Phys. **46**, 810 (1975).
[4]A. H. Meitzler and H. M. O'Bryan, Jr., Proc. IEEE **61**, 959 (1973).
[5]K. Carl and K. Geisen, Proc. IEEE **61**, 967 (1973).
[6]D. Viehland, J. F. Li, S. J. Jang, L. E. Cross, and M. Wuttig, Phys. Rev. B **46**, 8013 (1992).
[7]C. A. Randall, A. S. Bhalla, T. R. Shrout, and L. E. Cross, J. Mater. Res. **5**, 829 (1990).
[8]L. Neel, Compt. R. Acad. Sci. **228**, 664 (1949).
[9]J. Kobayashi and Y. Uesu, J. Appl. Crystallogr. **16**, 204 (1983).
[10]J. Kobayashi, H. Kumomi, and K. Saito, J. Appl. Crystallogr. **19**, 377 (1986).
[11]J. Kobayashi, T. Asahi, S. Takahashi, and A. M. Glazer, J. Appl. Crystallogr. **21**, 479 (1988).
[12]For instances, Refs. 1, 5, and C. J. Kirkby, Ferroelectrics **37**, 567 (1981).
[13]M. Yokosuka and M. Marutake, Jpn. J. Appl. Phys. **25**, 981 (1986).
[14]J. Harada, T. Pedersen, and Z. Barnea, Acta Crystallogr. Sec. A **26**, 336 (1970).
[15]A. F. Devonshire, Philos. Mag. **42**, 1040 (1949).
[16]W. A. Schulze, J. V. Biggers, and L. E. Cross, J. Am. Ceram. Soc. **61**, 46 (1978).
[17]D. Schwarzenbach, Z. Kristallogr. **123**, 161 (1966).
[18]M. V. Hobden, Nature (London) **216**, 678 (1967).
[19]J. Kobayashi, J. Bouillot, and K. Kinoshita, Phys. Status Soli-

di B **47**, 619 (1971).
[20]B. Ayrault, F. Lefin, H. Langlois, Y. Toudic, and J. F. Palmier, Opt. Commun. **5**, 239 (1972).
[21]S. C. Abrahams, C. Svensson, and A. R. Tanguay, Jr., Solid State Commun. **30**, 293 (1979).
[22]K. Stadnicka, A. M. Glazer, and J. R. L. Moxon, J. Appl. Crystallogr. **18**, 237 (1985).
[23]K. A. McCarthy, A. P. Goutzoulis, M. Gottlieb, and N. B. Singh, Opt. Commun. **64**, 157 (1987).
[24]K. Saito, H. Sugiya, and J. Kobayashi, J. Appl. Phys. **68**, 732 (1987).
[25]J. Kobayashi, K. Uchino, and T. Ashahi, Phys. Rev. B **43**, 5706 (1990).
[26]T. Asahi, M. Tomizawa, J. Kobayashi, and W. Kleemann, Phys. Rev. B **45**, 1971 (1992).
[27]K. Saito and J. Kobayashi, Phys. Rev. B **45**, 10 264 (1992).
[28]J. Kobayashi, K. Uchino, H. Matsuyama, and K. Saito, J. Appl. Phys. **69**, 409 (1991).
[29]K. Saito, F. T. Cao, and J. Kobayashi, Jpn. J. Appl. Phys. **31**, 3225 (1992).
[30]J. Kobayashi, T. Asahi, and S. Takahashi, Ferroelectrics **75**, 139 (1987).
[31]K. Saito, T. Kawabe, and J. Kobayashi, Ferroelectrics **75**, 153 (1987).
[32]K. Matsuda, H. Sugiya, and J. Kobayashi, Ferroelectrics **107**, 39 (1990).
[33]N. Takahashi, M. Tomizawa, and J. Kobayashi, Jpn. J. Appl. Phys. **31**, 3209 (1992).
[34]A. R. Johnston and J. M. Weingar, J. Opt. Soc. Am. **55**, 828 (1965).
[35]J. D. Zook, D. Chen, and G. N. Otto, Appl. Phys. Lett. **11**, 159 (1967).
[36]P. V. Lenzo, E. H. Turner, E. G. Spencer, and A. A. Ballman, Appl. Phys. Lett. **8**, 81 (1966).

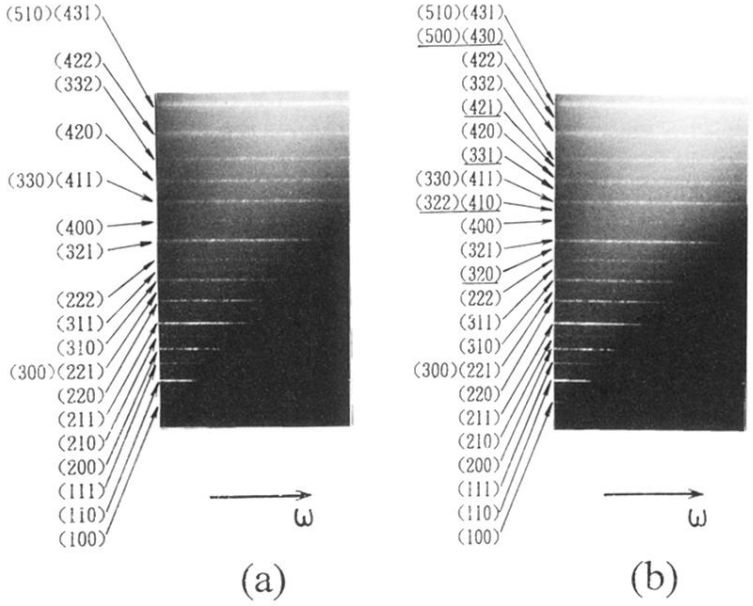

FIG. 5. Weissenberg photographs of PLZT(8/70/30) at (a) 90 °C and (b) −30 °C.